

# Production of a Chiral Magnetic Anomaly with Emerging Turbulence and Mean-Field Dynamo Action

Jennifer Schober,<sup>1,\*</sup> Igor Rogachevskii,<sup>2,3</sup> and Axel Brandenburg<sup>3,4,5,6</sup>

<sup>1</sup>*Laboratoire d'Astrophysique, EPFL, CH-1290 Sauverny, Switzerland*

<sup>2</sup>*Department of Mechanical Engineering, Ben-Gurion University of the Negev, P.O. Box 653, Beer-Sheva 84105, Israel*

<sup>3</sup>*Nordita, KTH Royal Institute of Technology and Stockholm University, 10691 Stockholm, Sweden*

<sup>4</sup>*The Oskar Klein Centre, Department of Astronomy,*

*Stockholm University, AlbaNova, SE-10691 Stockholm, Sweden*

<sup>5</sup>*School of Natural Sciences and Medicine, Ilia State University, 0194 Tbilisi, Georgia*

<sup>6</sup>*McWilliams Center for Cosmology and Department of Physics, Carnegie Mellon University, Pittsburgh, Pennsylvania 15213, USA*

(Dated: February 15, 2022)

In relativistic magnetized plasmas, asymmetry in the number densities of left- and right-handed fermions, i.e., a nonzero chiral chemical potential  $\mu_5$ , leads to an electric current along the magnetic field. This causes a chiral dynamo instability for a uniform  $\mu_5$ , but our simulations reveal a dynamo even for fluctuating  $\mu_5$  with zero mean. It produces magnetically dominated turbulence and generates mean magnetic fields via the magnetic  $\alpha$  effect. Eventually, a universal scale-invariant  $k^{-1}$  spectrum of  $\mu_5$  and a  $k^{-3}$  magnetic spectrum are formed independently of the initial condition.

The chiral magnetic effect (CME) is a macroscopic quantum phenomenon. It leads to an electric current along the magnetic field due to an imbalance between oppositely handed electrically charged fermions [1]. This is a direct consequence of the coupling of fermionic chirality and the topology of magnetic field lines characterized by magnetic helicity [2, 3]. Chiral asymmetry is quantified by the chiral chemical potential  $\mu_5 \equiv \mu_L - \mu_R$ , which is nonzero in regions where the chemical potentials of left- ( $\mu_L$ ) and right-handed ( $\mu_R$ ) fermions differ. It has been shown [4] that  $\mu_5$  can survive down to energies of  $\approx 10$  MeV and thereby the CME can potentially affect leptogenesis during the QCD phase transition [5] and produce gravitational waves in the early Universe [6].

The dynamics of chiral fluids has been studied in various approaches [4, 7–12], including an effective description called chiral magnetohydrodynamics (MHD) [13–16]. A significant difference to classical MHD is that the CME can induce a dynamo instability in the magnetic field on small length scales [17]. Unlike classical MHD dynamos, chiral dynamos can occur without an initial velocity field and self-consistently produce turbulence through the Lorentz force. This can activate a chiral mean-field dynamo [14, 18–20].

The possibility of efficient magnetic field amplification through the CME has relevance for the early Universe. In particular, the transport of magnetic energy to large length scales via a chiral inverse cascade [4, 21–23] and the chiral mean-field dynamo, strongly increases the chance of primordial magnetic fields [24, 25] to survive until present day. Thereby, observational constraints on magnetic fields in cosmic voids [26] may open up a unique window into the fundamental physics of the early Universe. Beyond cosmology, chiral MHD has also relevance to neutron stars [27–31], quark-gluon plasmas in heavy-ion collisions [2, 3, 32], and quantum materials [33].

In all previous chiral dynamo studies, a uniform initial  $\mu_5$  has been considered [14, 18–20]. However, a uniform  $\mu_5$  requires special generation mechanisms. Therefore, we consider in this Letter a more general and universal situation with initial fluctuations of the chiral chemical potential, but zero mean.

For the analysis, we normalize  $\mu_5$  by  $4\alpha_{\text{em}}/(\hbar c)$  such that it has the dimension of inverse length, where  $\alpha_{\text{em}}$  is the fine structure constant,  $c$  is the speed of light, and  $\hbar$  is the reduced Planck constant. The strength of the coupling of the electromagnetic field to  $\mu_5$  is characterized by the chiral feedback parameter  $\lambda$  which, for hot plasmas, is given by  $\lambda = 3\hbar c(8\alpha_{\text{em}})^2/(k_B T)^2$ , where  $T$  is the temperature and  $k_B$  is the Boltzmann constant. We consider the following set of chiral MHD equations [14]:

$$\frac{\partial \mathbf{B}}{\partial t} = \nabla \times [\mathbf{U} \times \mathbf{B} - \eta (\nabla \times \mathbf{B} - \mu_5 \mathbf{B})], \quad (1)$$

$$\rho \frac{D\mathbf{U}}{Dt} = (\nabla \times \mathbf{B}) \times \mathbf{B} - \nabla p + \nabla \cdot (2\nu \rho \mathbf{S}), \quad (2)$$

$$\frac{D\rho}{Dt} = -\rho \nabla \cdot \mathbf{U}, \quad (3)$$

$$\frac{D\mu_5}{Dt} = \mathcal{D}_5(\mu_5) + \lambda \eta [\mathbf{B} \cdot (\nabla \times \mathbf{B}) - \mu_5 \mathbf{B}^2], \quad (4)$$

where the magnetic field  $\mathbf{B}$  is normalized such that the magnetic energy density is  $\mathbf{B}^2/2$ , and  $D/Dt = \partial/\partial t + \mathbf{U} \cdot \nabla$  with  $\mathbf{U}$  being the velocity field. Further,  $\eta$  is the microscopic magnetic diffusivity,  $p$  is the fluid pressure,  $S_{ij} = (U_{i,j} + U_{j,i})/2 - \delta_{ij}(\nabla \cdot \mathbf{U})/3$  are the components of the trace-free strain tensor  $\mathbf{S}$  (commas denote partial spatial derivatives) and  $\nu$  is the kinematic viscosity. We adopt an isothermal equation of state,  $p = \rho c_s^2$ , with  $c_s$  being the sound speed. Equations (1)–(4) imply that total chirality  $\chi_{\text{tot}} \equiv \langle \mathcal{H} \rangle + 2\langle \mu_5 \rangle/\lambda$  is conserved, where angle brackets denote volume averaging. Here,  $\langle \mathcal{H} \rangle \equiv \langle \mathbf{A} \cdot \mathbf{B} \rangle$  is the magnetic helicity with the vector potential  $\mathbf{A}$  and  $\mathbf{B} = \nabla \times \mathbf{A}$ .

TABLE I. Summary of all runs.

Run	$E_5(k, t_0)$	$\mu_{5,\text{rms}}(t_0)$	$\mu_{5,\text{max}}(t_0)$	$\mu_{5,\text{max}}(t_5)$	$\max(\text{Re}_M)$
R-2	$\propto k^{-2}$	13.8	50.5	48.1	288
R-1	$\propto k^{-1}$	15.8	85.8	62.0	134
R+1	$\propto k^1 e^{-(k/10)^2}$	12.6	53.7	53.7	65.1

At the initial time  $t_0$ , we assume  $\langle \mu_5 \rangle(t_0) = 0$ , but nonzero fluctuations,  $\mu'_5$ , i.e.,  $\langle \mu_5'^2 \rangle(t_0) \neq 0$ . Initially, small fluctuations of  $\mathbf{B}$  with zero mean are present, while the velocity field vanishes. The fluctuations  $\mu'_5$  result in an exponential growth of magnetic fluctuations due to the chiral dynamo. This instability is caused by the term  $\nabla \times (v_5 \mathbf{B})$  in Eq. (1) with  $v_5 = \eta \mu_5$  and has a growth rate  $\gamma(k) = |v_5|k - \eta k^2$ , with  $k$  being the wave number. This instability is referred to as the chiral dynamo [17] and occurs when  $|v_5| > \eta k$ . Its maximum growth rate is  $\gamma_5 = v_5^2/4\eta$  and is attained at  $k_5 = |\mu_5|/2$ . We note that, while the  $\nabla \times (v_5 \mathbf{B})$  term in Eq. (1) is formally similar to the kinetic  $\alpha$  effect in classical mean-field MHD [14], the velocity  $v_5$  is not produced by helical turbulence, but rather by the CME. During the chiral dynamo phase, magnetic fluctuations produce velocity fluctuations via the Lorentz force  $(\nabla \times \mathbf{B}) \times \mathbf{B}$ .

Since the initial mean chiral chemical potential is zero, and the initial small-scale magnetic helicity  $\langle \mathbf{a} \cdot \mathbf{b} \rangle(t_0)$  related to the fluctuations of the vector potential  $\mathbf{a}$  and the magnetic field  $\mathbf{b}$  vanishes, we have  $\chi_{\text{tot}}(t_0) = 0$ . The initial  $\mu'_5$  with a wide range of scales produces  $\mathbf{b}$  by the chiral dynamo. Indeed, for a wide spectrum in  $k$  space, fluctuations of  $\mu_5$  on larger scales serve as a *mean field* for fluctuations on smaller scales, so that the chiral dynamo instability excites  $\mathbf{b}$  and produces small-scale magnetic helicity  $\langle \mathbf{a} \cdot \mathbf{b} \rangle$ . Because of the conservation of total chirality,  $\chi_{\text{tot}}(t) = 0$ , the generation of  $\langle \mathbf{a} \cdot \mathbf{b} \rangle$  causes growth of the mean chiral chemical potential,  $\langle \mu_5 \rangle = -\lambda \langle \mathbf{a} \cdot \mathbf{b} \rangle / 2$ . Simultaneously, the chiral dynamo drives turbulence magnetically and therefore enhances the fluid and magnetic Reynolds numbers,  $\text{Re} \equiv U_{\text{rms}}/(\nu k_{\text{int}})$  and  $\text{Re}_M \equiv U_{\text{rms}}/(\eta k_{\text{int}})$ , where  $k_{\text{int}}^{-1}$  is the integral scale of magnetically driven turbulence. When  $\text{Re}_M$  is large enough, the mean-field dynamo instability is excited and amplifies a large-scale magnetic field. These theoretical ideas are now checked in DNS.

We use the PENCIL CODE [34] to solve Eqs. (1)–(4) with high-order finite difference methods in a 3D periodic domain of size  $L^3 = (2\pi)^3$  with a resolution of  $672^3$ . The smallest wave number covered in the numerical domain is  $k_1 = 2\pi/L = 1$  which we use for normalization of length scales. All velocities are normalized to  $c_s = 1$  and the mean fluid density is  $\bar{\rho} = 1$ . Time is expressed in terms of the resistive time  $t_\eta = (\eta k_1^2)^{-1}$  with  $\eta$  being the microscopic diffusivity, which is a relevant constant throughout the DNS. We stress, however, that in magnetically driven turbulence, turbulent diffusion dom-

inates shortly after the onset of the mean-field dynamo, yet it is not practical for normalization due to its time dependence.

For numerical stability, diffusion of  $\mu_5$  has to be applied in Eq. (4). To affect primarily the largest resolved wave numbers  $k$  in the simulation domain, we use hyperdiffusion,  $\mathcal{D}_5(\mu_5) = -\mathcal{D}_5 \nabla^4 \mu_5$ ; see the companion paper [35] for technical details. In all runs, we use  $\nu = \eta = 2 \times 10^{-4}$ , i.e.  $\text{Re}_M = \text{Re}$ , which are based on the time-dependent integral scale of magnetically driven turbulence,

$$k_{\text{int}}^{-1} \equiv \frac{\int_1^{k_{\text{max}}} E_M(k) k^{-1} dk}{\int_1^{k_{\text{max}}} E_M(k) dk}. \quad (5)$$

Here,  $E_M$  is the magnetic energy spectrum, scaled such that  $\int_0^{k_{\text{max}}} E_M(k, t) dk \equiv \langle \mathbf{B}^2 \rangle / 2$ . Likewise, power spectra of  $\mu_5$  obey  $\int_0^{k_{\text{max}}} E_5(k, t) dk \equiv \langle \mu_5^2 \rangle$ . As initial conditions we use  $\mathbf{U} = \mathbf{0}$  and a weak seed magnetic field in form of Gaussian noise. Initial fluctuations of  $\mu_5$  are also set up as Gaussian noise, but with a specific spectrum that follows a power law in  $k$  space, i.e.,  $E_5(t_0) = E_{5,0} (k/k_1)^s \exp(-k^2/k_{\text{cut}}^2)$  with a cutoff  $k_{\text{cut}}$  that is needed for  $s > -1$ . We perform runs with  $s = -2, -1, +1$  (see Table I) and the amplitude  $E_{5,0}$  is chosen such that the maximum value of  $\mu_5$  in the domain is comparable for all runs at the time  $t_5$  when the chiral dynamo starts. In all runs, the initial mean value of  $\mu_5$  is vanishing, so that  $\chi_{\text{tot}} = \langle \mathcal{H} \rangle + 2\langle \mu_5 \rangle / \lambda \approx 0$ , and we use  $\lambda = 400$ .

The fluctuations  $\mu'_5$  result in an exponential growth of  $B_{\text{rms}}$  at the rate  $\gamma_5$  due to the chiral dynamo, as can be seen in Fig. 1a. Usage of  $v_5 = \eta \mu_{5,\text{max}}$  in the expression for  $\gamma_5$  with the maximum value of the chiral chemical potential,  $\mu_{5,\text{max}}$ , as shown in Fig. 1b, reproduces the observed growth rate for all runs rather well; see Fig. 1c (and Fig. 3b). We note, however, that a sufficient separation of scales is required for the dynamo to reach the maximum possible growth rate; see the accompanying paper [35]. When comparing the measured growth rate with  $\gamma_5$ , we neglect the change of  $\mu_5$  in time, which is much smaller than the increase of  $B_{\text{rms}}$ . During the chiral dynamo phase,  $\langle \mathcal{H} \rangle$  (Fig. 1a) and  $\langle \mu_5 \rangle$  [Fig. 1b] are produced. If the divergence of magnetic helicity fluxes is small, the latter two always tend to have opposite signs, as follows from the conservation of total chirality. Therefore, contrary to previously considered cases with an initially uniform  $\mu_5$ , the conservation law cannot be used to estimate the maximum magnetic field produced by the chiral dynamo.

With magnetic field amplification via the chiral dynamo, velocity fluctuations are produced by the Lorentz force. When the turbulent velocity approaches the Alfvén speed,  $U_{\text{rms}} \approx v_A \equiv B_{\text{rms}}$  (at  $t \approx 0.03$  for run R+1 and  $t \approx 0.05$  for runs R-2 and R-1) the small-scale chiral dynamo phase ends. This coincides with the time  $t_{\text{IC}}$  when the peak of the magnetic energy spectrum reaches

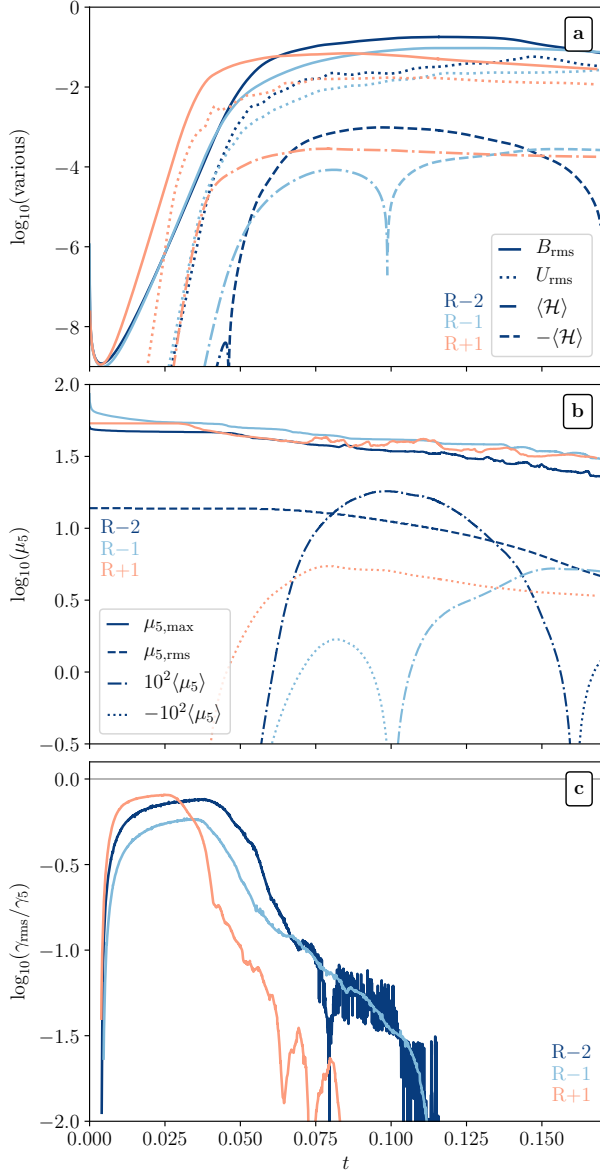


FIG. 1. Direct comparison between the time evolution of different quantities of all simulations. Different colors refer to different runs: R-2 (dark blue), R-1 (light blue), and R+1 (orange). (a) Time series of  $B_{\text{rms}}$ ,  $U_{\text{rms}}$ , and  $\langle \mathcal{H} \rangle$ . (b) Time series of  $\mu_{5,\max}$  and  $\langle \mu_5 \rangle$ . The latter has been multiplied by a factor of 100 for better visualization. (c) Measured growth rate of  $B_{\text{rms}}$ ,  $\gamma_{\text{rms}}$ , over  $\gamma_5 = \eta \mu_{5,\max}^2/4$ .

$\eta^2 \mu_{5,\max}(t_0)$  and starts to shift to larger scales; see  $E_M$  for run R-2 in Fig. 2a.

In such chiral-magnetically driven turbulence, a mean-field dynamo instability can occur if  $\text{Re}$  and  $\text{Re}_M$  are large. To study the mean-field dynamo, we perform averages  $\langle \mu_5 \rangle_{\text{int}}$ ,  $\langle B \rangle_{\text{int}}$ , and  $\langle \mathcal{H} \rangle_{\text{int}}$  on the scale  $k_{\text{int}}$  (see Fig. 2b), defined as

$$\langle X \rangle_{\text{int}} = \left[ \frac{\int_0^{k_{\text{max}}} E_M(k) E_X(k) dk}{\int_0^{k_{\text{max}}} E_M(k) dk} \right]^{1/2}, \quad (6)$$

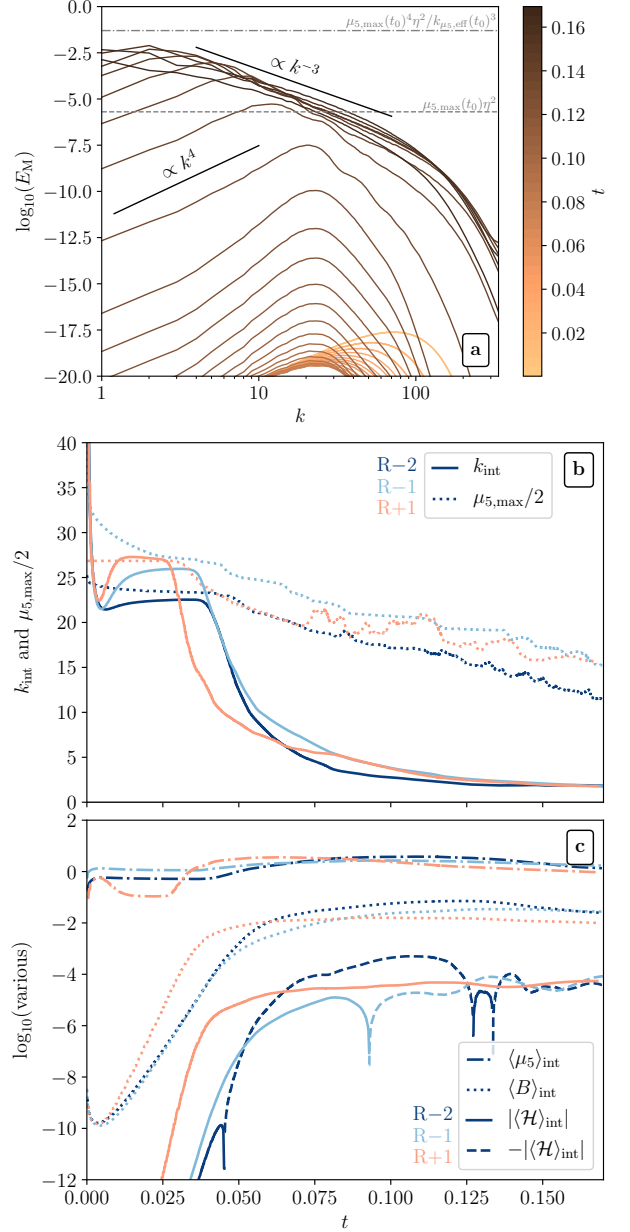


FIG. 2. (a) Time evolution of the magnetic energy spectrum  $E_M$  for run R-2 with time indicated by the color bar. (b) The wave number based on the integral scale of turbulence,  $k_{\text{int}}$ , as a function of time for all runs (solid lines) and the value of the theoretically predicted wave number,  $\mu_{5,\max}/2$ , on which the  $v_5$  dynamo instability has the largest growth rate (dotted lines). (c) Different averages based on the  $k_{\text{int}}$ :  $\langle \mu_5 \rangle_{\text{int}}$  (dashed-dotted),  $\langle B \rangle_{\text{int}}$  (dotted lines),  $\langle \mathcal{H} \rangle_{\text{int}}$  (solid lines), and  $-\langle \mathcal{H} \rangle_{\text{int}}$  (dashed lines).

where  $E_X(k)$  is the spectrum of  $X$ ; see Fig. 2c.

The mean-field dynamo instability has a maximum growth rate of  $\gamma_\alpha = (\eta \langle \mu_5 \rangle_{\text{int}} + \alpha_\mu + \alpha_M + \alpha_K)^2 / (4\eta_T)$ , where  $\eta_T \approx U_{\text{rms}} / (3k_{\text{int}})$  is the turbulent magnetic diffusivity. The different  $\alpha$  effects are approximately given by  $\alpha_\mu = -(2/3)\eta \langle \mu_5 \rangle_{\text{int}} \log(\text{Re}_M)$  [14],  $\alpha_M = 2(q-1)/(q+1)\tau_c \chi_c$ , and  $\alpha_K = -(1/3)\tau_c \chi_K$ . Here,  $\chi_c =$

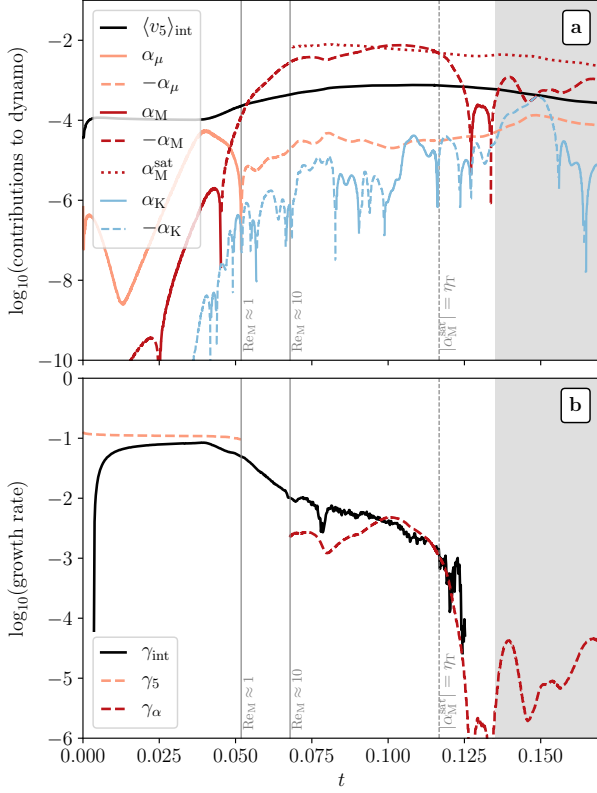


FIG. 3. Time evolution of different quantities in Run R-2. Gray background indicates that the inverse cascade has reached the size of the domain. (a) Different contributions to the mean-field dynamo growth rate, including  $\langle v_5 \rangle_{\text{int}} \equiv \eta \langle \mu_5 \rangle_{\text{int}}$ . (b) The measured growth rate of  $\langle B \rangle_{\text{int}}$ ,  $\gamma_{\text{int}}$  (black solid line) compared to the chiral dynamo growth rate  $\gamma_5$  (orange dashed line) and the mean-field dynamo growth rate  $\gamma_\alpha$  based on  $\alpha_M$  (red dashed line).

$\langle \mathbf{b} \cdot (\nabla \times \mathbf{b}) \rangle_{\text{int}} \approx \langle \mathbf{a} \cdot \mathbf{b} \rangle_{\text{int}} k_{\text{int}}^2$  is the current helicity,  $\chi_K = \langle \mathbf{u} \cdot \boldsymbol{\omega} \rangle_{\text{int}}$  is the kinetic helicity,  $\boldsymbol{\omega} \equiv \nabla \times \mathbf{u}$  is the vorticity,  $\tau_c \approx (v_A k_{\text{int}})^{-1}$  is the correlation time of magnetically driven turbulence, and  $q$  is the slope of the magnetic energy spectrum  $\propto k^{-q}$ . We use  $q = 3$ ; see Fig. 2a. Figure 3a shows that  $\alpha_M$  dominates once turbulence is produced and therefore the mean-field dynamo growth rate is  $\gamma_\alpha \approx \alpha_M^2 / (4\eta_T)$ .

Our DNS indicate that  $\chi_c$  plays the key role for the mean-field dynamo sourced by initially inhomogeneous fluctuations of  $\mu_5$ ; see Fig. 3a and the accompanying paper [35]. The evolution of  $\chi_c$  is closely connected to that of the small-scale magnetic helicity [14]:

$$\frac{\partial}{\partial t} \overline{\mathbf{a} \cdot \mathbf{b}} + \text{div } \mathbf{F} = 2\overline{v_5 \mathbf{b}^2} - 2\overline{\boldsymbol{\mathcal{E}} \cdot \mathbf{B}} - 2\eta_T \overline{\mathbf{b} \cdot (\nabla \times \mathbf{b})}, \quad (7)$$

where  $\overline{\boldsymbol{\mathcal{E}}} \equiv \overline{\mathbf{u} \times \mathbf{b}} = \alpha_M \overline{\mathbf{B}} - \eta_T (\nabla \times \overline{\mathbf{B}})$  is the electromotive force with  $\alpha_M$  being the dominant contribution to the total  $\alpha$  effect, and  $\mathbf{F}$  is the flux of  $\mathbf{a} \cdot \mathbf{b}$ . Near magnetic field maximum, two leading source/sink terms in Eq. (7),  $2\overline{v_5 \mathbf{b}^2} - 2\alpha_M \overline{\mathbf{B}^2}$ , compensate each other, so that the magnetic  $\alpha$  effect reaches the value  $\alpha_M^{\text{sat}} = \eta \overline{\mu_5 \mathbf{b}^2} / \overline{\mathbf{B}^2}$ . For

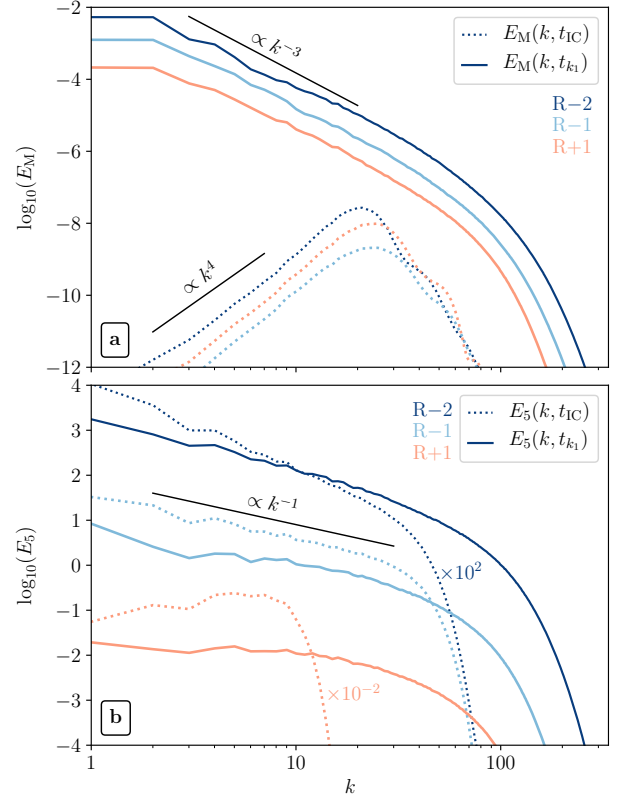


FIG. 4. Power spectra from all simulations. (a) Magnetic energy spectra  $E_M$  at the beginning of the chiral inverse cascade  $t_{\text{IC}}$  (dotted lines) and the time when the cascade reaches the size of the numerical domain  $t_{k_1}$  (solid lines). (b) Spectra of  $\mu_5$  shown at the same two characteristic times as  $E_M$ . For better visibility the spectra of runs R-2 and R+1 have been multiplied by factors of  $10^2$  and  $10^{-2}$ , respectively.

R-2,  $|\alpha_M| \approx |\alpha_M^{\text{sat}}|$  for  $t \gtrsim 0.075$ , as can be seen in Fig. 3a.

The maximum growth rate of the mean-field dynamo instability  $\gamma_\alpha$  agrees well with the measured growth rate  $\gamma_{\text{int}}$  of  $\langle B \rangle_{\text{int}}$ ; see Fig. 3b for run R-2 in the interval  $0.075 < t < 0.12$ . Since  $\chi_{\text{tot}}(t_0) = 0$ , the conservation law cannot be employed here to find the maximum magnetic field value; but see the companion paper [35] for a phenomenological model. In our DNS,  $\gamma_{\text{int}}$  strongly decreases when the scale at which  $\gamma_\alpha$  is maximum becomes larger than the size of the box. As can be seen in Fig. 3b,  $\gamma_{\text{int}}$  vanishes once the positive contribution to the growth rate on the minimum wave number of the box,  $|\alpha_M^{\text{sat}}| k_1$ , becomes comparable to the negative contribution,  $\eta_T k_1^2$ . For R-2, dissipation due to  $\eta_T k_1^2$  on the box scale dominates for  $t \gtrsim 0.12$ .

At the time  $t_{k_1}$  when the peak of the magnetic energy reaches the size of the domain, all of the  $\mu_5$  spectra approach a universal  $k^{-1}$ ; see Fig. 4. The magnetic energy spectra approach a  $k^{-3}$  scaling which is, for fully helical magnetic fields, consistent with the magnetic helicity spectra  $\propto k^{-4}$ .

In conclusion, a small-scale chiral dynamo can arise from an initially fluctuating chiral chemical potential with zero mean. The chiral dynamo generates small-scale magnetic helicity which (i) produces a mean  $\mu_5$  due to the conservation of total chirality and (ii) drives turbulence via the Lorentz force. In our DNS, sufficiently strong turbulence is generated to activate a mean-field dynamo that is well described by the magnetic  $\alpha$  effect caused by current helicity. During the mean-field dynamo phase, the power spectra develop a universal shape;  $E_M \propto k^{-3}$  and  $E_5 \propto k^{-1}$ . In particular, with the onset of turbulence in the system,  $\mu_5$  becomes scale invariant, independent of its initial condition.

We have benefited from stimulating discussions with Abhijit B. Bendre, Nathan Kleeorin, and Matthias Rheinhardt. J.S. acknowledges the support by the Swiss National Science Foundation under Grant No. 185863. A.B. was supported in part through a grant from the Swedish Research Council (Vetenskapsrådet, 2019-04234).

---

\* jennifer.schober@epfl.ch

- [1] A. Vilenkin, Equilibrium parity violating current in a magnetic field, *Phys. Rev. D* **22**, 3080 (1980).
- [2] D. E. Kharzeev, The chiral magnetic effect and anomaly-induced transport, *Prog. Part. Nucl. Phys.* **75**, 133 (2014).
- [3] D. E. Kharzeev, J. Liao, S. A. Voloshin, and G. Wang, Chiral magnetic and vortical effects in high-energy nuclear collisions—A status report, *Progress in Particle and Nuclear Physics* **88**, 1 (2016).
- [4] A. Boyarsky, J. Fröhlich, and O. Ruchayskiy, Self-consistent evolution of magnetic fields and chiral asymmetry in the early Universe, *Phys. Rev. Lett.* **108**, 031301 (2012).
- [5] D. J. Schwarz and M. Stuke, Lepton asymmetry and the cosmic QCD transition, *J. Cosmol. Astropart. Phys.* **11**, 025 (2009).
- [6] A. Brandenburg, Y. He, T. Kahniashvili, M. Rheinhardt, and J. Schober, Relic Gravitational Waves from the Chiral Magnetic Effect, *Astrophys. J.* **911**, 110 (2021).
- [7] D. G. Figueroa, A. Florio, and M. Shaposhnikov, Chiral charge dynamics in Abelian gauge theories at finite temperature, *Journal of High Energy Physics* **2019**, 142 (2019).
- [8] M. Mace, N. Mueller, S. Schlichting, and S. Sharma, Chiral instabilities and the onset of chiral turbulence in QED plasmas, *Phys. Rev. Lett.* **124**, 191604 (2020).
- [9] M. A. Stephanov and Y. Yin, Chiral Kinetic Theory, *Phys. Rev. Lett.* **109**, 162001 (2012).
- [10] J.-Y. Chen, D. T. Son, and M. A. Stephanov, Collisions in chiral kinetic theory, *Phys. Rev. Lett.* **115**, 021601 (2015).
- [11] E. V. Gorbar, I. A. Shovkovy, S. Vilchinskii, I. Rudenok, A. Boyarsky, and O. Ruchayskiy, Anomalous Maxwell equations for inhomogeneous chiral plasma, *Phys. Rev. D* **93**, 105028 (2016).
- [12] N. Yamamoto and D.-L. Yang, Chiral Radiation Transport Theory of Neutrinos, *Astrophys. J.* **895**, 56 (2020).
- [13] M. Giovannini, Anomalous magnetohydrodynamics, *Phys. Rev. D* **88**, 063536 (2013).
- [14] I. Rogachevskii, O. Ruchayskiy, A. Boyarsky, J. Fröhlich, N. Kleeorin, A. Brandenburg, and J. Schober, Laminar and turbulent dynamos in chiral magnetohydrodynamics I: Theory, *Astrophys. J.* **846**, 153 (2017).
- [15] L. Del Zanna and N. Bucciantini, Covariant and 3+1 equations for dynamo-chiral general relativistic magnetohydrodynamics, *Monthly Not. Roy. Astron. Soc.* **479**, 657 (2018).
- [16] K. Hattori, Y. Hirono, H.-U. Yee, and Y. Yin, Magnetohydrodynamics with chiral anomaly: Phases of collective excitations and instabilities, *Phys. Rev. D* **100**, 065023 (2019).
- [17] M. Joyce and M. Shaposhnikov, Primordial magnetic fields, right electrons, and the Abelian anomaly, *Phys. Rev. Lett.* **79**, 1193 (1997).
- [18] J. Schober, I. Rogachevskii, A. Brandenburg, A. Boyarsky, J. Fröhlich, O. Ruchayskiy, and N. Kleeorin, Laminar and Turbulent Dynamos in Chiral Magnetohydrodynamics II. Simulations, *Astrophys. J.* **858**, 124 (2018).
- [19] J. Schober, A. Brandenburg, I. Rogachevskii, and N. Kleeorin, Energetics of turbulence generated by chiral mhd dynamos, *Geophys. Astrophys. Fluid Dyn.* **113**, 107 (2019).
- [20] J. Schober, A. Brandenburg, and I. Rogachevskii, Chiral fermion asymmetry in high-energy plasma simulations, *Geophys. Astrophys. Fluid Dyn.* **114**, 106 (2020).
- [21] Y. Hirono, D. E. Kharzeev, and Y. Yin, Self-similar inverse cascade of magnetic helicity driven by the chiral anomaly, *Phys. Rev. D* **92**, 125031 (2015).
- [22] E. V. Gorbar, I. Rudenok, I. A. Shovkovy, and S. Vilchinskii, Anomaly-driven inverse cascade and inhomogeneities in a magnetized chiral plasma in the early universe, *Phys. Rev. D* **94**, 103528 (2016).
- [23] A. Brandenburg, J. Schober, I. Rogachevskii, T. Kahniashvili, A. Boyarsky, J. Fröhlich, O. Ruchayskiy, and N. Kleeorin, The turbulent chiral-magnetic cascade in the early Universe, *Astrophys. J. Lett.* **845**, L21 (2017).
- [24] K. Subramanian, The origin, evolution and signatures of primordial magnetic fields, *Rep. Prog. Phys.* **79**, 076901 (2016).
- [25] T. Vachaspati, Progress on cosmological magnetic fields, *Reports on Progress in Physics* **84**, 074901 (2021).
- [26] A. Neronov and I. Vovk, Evidence for strong extragalactic magnetic fields from Fermi observations of TeV blazars, *Science* **328**, 73 (2010).
- [27] M. Dvornikov and V. B. Semikoz, Magnetic helicity evolution in a neutron star accounting for the Adler-Bell-Jackiw anomaly, *J. Cosmol. Astropart. Phys.* **2018** (08), 021.
- [28] Y. Masada, K. Kotake, T. Takiwaki, and N. Yamamoto, Chiral magnetohydrodynamic turbulence in core-collapse supernovae, *Phys. Rev. D* **98**, 083018 (2018).
- [29] N. Yamamoto, Chiral transport of neutrinos in supernovae: Neutrino-induced fluid helicity and helical plasma instability, *Phys. Rev. D* **93**, 065017 (2016).
- [30] G. Sigl and N. Leite, Chiral magnetic effect in protoneutron stars and magnetic field spectral evolution, *J. Cosmol. Astropart. Phys.* **1**, 025 (2016).
- [31] M. Dvornikov, V. B. Semikoz, and D. D. Sokoloff, Generation of strong magnetic fields in a nascent neutron star

- accounting for the chiral magnetic effect, *Phys. Rev. D* **101**, 083009 (2020).
- [32] Y. Hirono, D. E. Kharzeev, and Y. Yin, New quantum effects in relativistic magnetohydrodynamics, *Nuclear Phys. A* **967**, 840 (2017).
- [33] V. Galitski, M. Kargarian, and S. Syzranov, Dynamo Effect and Turbulence in Hydrodynamic Weyl Metals, *Phys. Rev. Lett.* **121**, 176603 (2018).
- [34] Pencil Code Collaboration, A. Brandenburg, A. Johansen, P. Bourdin, W. Dobler, W. Lyra, M. Rheinhardt, S. Bingert, N. Haugen, A. Mee, F. Gent, N. Babkovskaia, C.-C. Yang, T. Heinemann, B. Dintrans, D. Mitra, S. Candelaresi, J. Warnecke, P. Käpylä, A. Schreiber, P. Chatterjee, M. Käpylä, X.-Y. Li, J. Krüger, J. Aarnes, G. Sarson, J. Oishi, J. Schober, R. Plasson, C. Sandin, E. Karchniwy, L. Rodrigues, A. Hubbard, G. Guerrero, A. Snodin, I. Losada, J. Pekkilä, and C. Qian, The Pencil Code, a modular MPI code for partial differential equations and particles: multipurpose and multiuser-maintained, *The Journal of Open Source Software* **6**, 2807 (2021).
- [35] J. Schober, I. Rogachevskii, and A. Brandenburg, companion paper, Dynamo instabilities in plasmas with inhomogeneous chiral chemical potential, *Phys. Rev. D* **105**, 043507 (2022).